Numerical Investigation of Transitional Effects in Critical Venturi Nozzles

E. von Lavante, B. Mickan* and R. Kramer***

*PTB, D-52133 Braunschweig, Germany

**Institute of Turbomachinery, University of Essen, D-45127 Essen, Germany

Abstract - Several Venturi nozzles, operating at critical conditions and shaped according to the recommendations of the ISO Standard 9300 were selected for the present study. The flow in the nozzles was investigated numerically for a range of Reynolds numbers. The present results were compared with experimental data where available. The unsteady compressible viscous flow in the nozzles was simulated using the Navier-Stokes solver ACHIEVE, developed by the first author. Several models for predicting the laminar-turbulent transition were tested. Significant phenomena associated with the transition were observed, having an influence on the discharge coefficient C_D.

I. INTRODUCTION

One of the simplest methods of highly accurate measurement of mass flows is the employment of critical nozzles. As a matter of fact, sonic nozzle test rigs are often used as reference flow meters [4], [5], [6], [7]. The guidelines and standards in using these devices are well defined and covered by the ISO Standard 9300 [8]. It is valid for toroidal nozzles with critical Reynolds numbers between $Re = 10^5$ and $Re = 10^7$. However, critical nozzles of significantly smaller diameter are also in frequent use [4], [5], [11]. In this case, relatively large fluctuations in the mass flow have been observed, making the calibration of these nozzles difficult. In particular, nozzles of diameters less than 1 mm and Reynolds numbers as small as $3 \cdot 10^3$ display higher measurement uncertainties.

In the past, flows in supersonic and transonic nozzles have been studied quite extensively. Due to their significant importance to the aerospace engineering, especially in the area of rocket propulsion, they were investigated numerically and experimentally numerous times [1], [12], [2]. However, most of the above research work concentrated on the overall features of these nozzles, assuming steady flow and leaving out some of the unsteady details.

In the recent past, the flow field in the sonic nozzles has been studied in more detail. Ishibashi et. al. [10] have shown results of combined experimental and numerical work that dealt with the shock structure, the boundary layer (BL) thickness and the velocity profiles in general in a typical nozzle designed according to the ISO 9300 standard. Further development of analytical methods used to compute the C_D -coefficient have been introduced in [17] for the case of laminar boundary layers. Flow instabilities and their effect on the C_D -coefficient have been numerically simulated by von Lavante et. al. [9]. An irregular choking phenomena have been studied by Nakao [15]. Although all the work described here contributed to better understanding of the flow in critical Venturi-Nozles, there have been several contibutions that indicated erratic behavior of the flow in Reynolds-number ranges between approximately $6 \cdot 10^5$ and $1.2 \cdot 10^6$. Typical in this regard is the plot of the C_D -coefficient published by Vallet et. al. [20] and shown in Fig. 1. Noticable is the sudden change of the slope of the C_D -coefficient ("jump"), coupled with a local decrease of its value and a change of the dependence on the Reynolds number.

Similar tendency has been also described by Ishibashi [21]. His results, augmented by additional data and theoretical curves of the dependence of C_D on the Reynolds number can be seen in Fig. 2.

The suspected cause for this behavior is the transition of the boundary layer from laminar to turbulent. Generally, the C_D -coefficient is proportional to the Reynolds number according to

$$C_D = a + b \cdot (Re_{ISO})^a \qquad (1)$$

where $a = -0.5$ in the laminar case , being in good agreement with the simple boundary layer theory for flat plate according to Blasius, and $a = -0.2$ in the turbulent case.

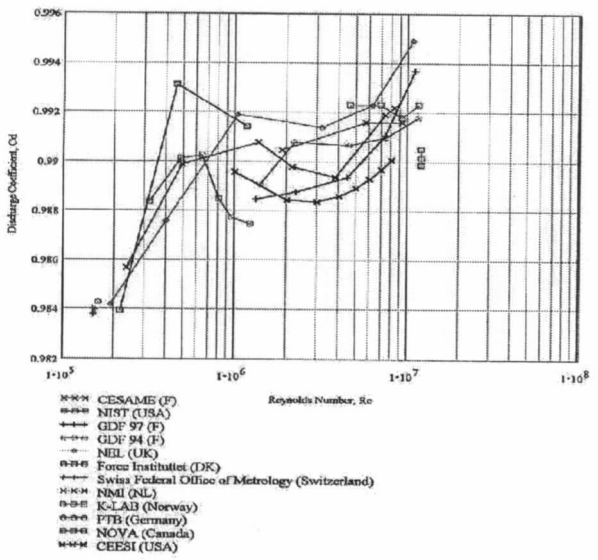

Figure 1: C_D -coefficient as a function of the Reynolds number, from [20].

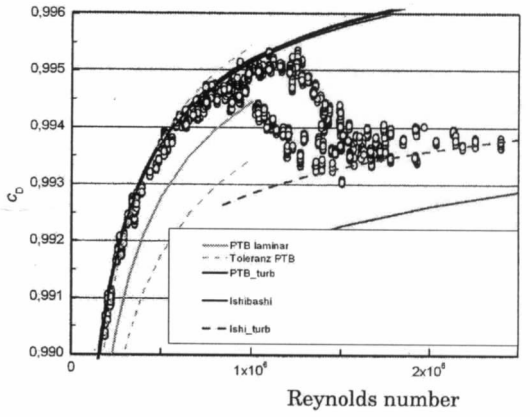

Figure 1: C_D -coefficient as a function of the Reynolds number, from [21].

The aim of the present research is to investigate the flow behavior in sonic nozzle test rigs with emphasis to the transition of the boundary layer flow from laminar to turbulent. A representative critical nozzle geometry, as recommended by the ISO Standard 9300, was selected for the present investigation. The nozzle shape is shown in Fig. 3. It is a typical convergent-divergent nozzle, with a toroidal throat having a diameter of between 0.3 and 321 mm, and a divergent part with a divergence wall angle of 4 deg. The Reynolds number based on the ISO 9300 -definition was between $Re = 2.2 \cdot 10^4$ and $Re = 4.15 \cdot 10^6$. The nozzle wall was assumend to be perfectly smooth. After the simulation of the flow field converged to a periodic solution, several transion criteria were applied to obtain an estimated location of the transition. The resulting conclusions about the existance of the transition were compared with corresponding experimental data, presented in a companion contribution in these proceedings.

II. NUMERICAL ALGORITHM

The numerical method employed in the present flow simulations is part of a flow simulation system developed at the Institute of Turbomachinery at the University of Essen, called "ACHIEVE". It consists of an upwind solver of the Navier-Stokes equations, using the finite volume discretization. The governing equations to be solved in the present simulations are the two-dimensional or axisymmetric compressible Navier-Stokes equations. The governing equations are given in more detail by, for example, Steger [13] or von Lavante et. al. [12].

2.1 Numerical Scheme

Due to the complexity of the predicted flow, a simple numerical scheme with central spacial differences and artificial dissipation added explicitely was not suited for the present simulations. Therefore, the well known and proven Roe's Scheme [3] was employed. The numerical scheme is based on Roe's Flux Difference Splitting in finite volume form, as developed by von Lavante et.al. [12]. The method has been proven to be accurate and effective in the simulation of viscous flows with wide range of Mach numbers [1].

The simulations were carried out on structured grids. The mesh points were arranged according to an algebraic distribution and clustered at the solid walls to ensure enough gridpoints in the boundary layers. The domain was divided into several blocks to make the formulation of the boundary conditions and handling a complex geometry easier. Furthermore, the Multiblock-structure was necessary to compute the flow on parallel computers.

The present numerical scheme is described in more detail in a companion paper by von Lavante et. al. [18] in these proceedings; more comprehensive information about the numerical and mathematical aspects of the present algorithm is offerred in [19].

2.2 Discretization in Time

The governing equations were integrated in time by solving their semidiscrete form by means of either modified Runge-Kutta (R-K) time stepping or implicit symmetric Gauß-Seidel (SGS) relaxation method. In the present work, the two stage

version of the R-K procedure was utilized. The corresponding Runge-Kutta coefficients α_i were optimized by von Lavante et. al. [14] for maximum multigrid performance (damping of high frequencies). That optimization was done, however, using a linear hyperbolic model equations. In realistic applications, these coefficients worked fine for the inviscid Euler equations as well as for most viscous cases. The simple two stage R-K procedure was as efficient as the more frequently used four stage scheme, but required only one optimized coefficient, $\alpha_1 = 0.42$.

2.3 Boundary Conditions

The present boundary conditions were implemented with the help of dummy (ghost) cells. At the subsonic inflow boundary, a locally one-dimensional weakly non-reflective boundary condition, based on the isentropic theory of the Riemann problem, was used. The tangential velocity, incoming Riemann invariant, total pressure and entropy in the first ghost cell were specified. The outgoing Riemann invariant was extrapolated from the interior domain. At the subsonic outflow boundary, the static pressure was specified, subject to the fluctuations allowed by the non-reflective treatment. The remaining variables were extrapolated. At solid walls, the velocities were anti-reflected, resulting in zero velocity on the boundary. The static pressure and density were reflected, resulting in zero gradients of these variables at the wall (adiabatic wall). Finally, at the interzonal boundaries, the block grids were overlapping by two cells, providing smooth transitions of the dependant variables Q due to the present MUSCL extrapolation in the projection phase.

III. SIMULATION OF THE FLOW FIELD

The simulations of the flow field have been accomplished using the above algorithm on a computational grid shown in Fig. 3. The computational domain consisted of three blocks, each having approximately $8.5 \cdot 10^3$ cells. The grid block downstream of the nozzle exit was necessary in order to ensure realistic conditions at this location.

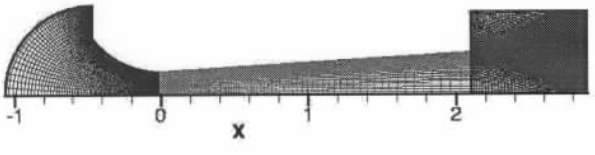

Figure 3: Computational grid.

In the present article, only the cases with ideal gas as the metered fluid will be discussed. Here, the gas was air at atmospheric conditions. The relatively large Reynolds number was accomplished by assuming a large throat diameter (up to 321 mm). In reality, the large Reynolds number was the result of high pressure level in the inflow. The outflow pressure ratio was assumed to be a constant $p_{out}/p_0 = 0.2$. This relatively low pressure ratio assured steady operating conditions in the throat. The contours of constant velocity magnitude and density in the resulting flow field are shown in Fig. 4 for the lower Reynolds number of $Re_{ISO} = 8.75 \cdot 10^5$.

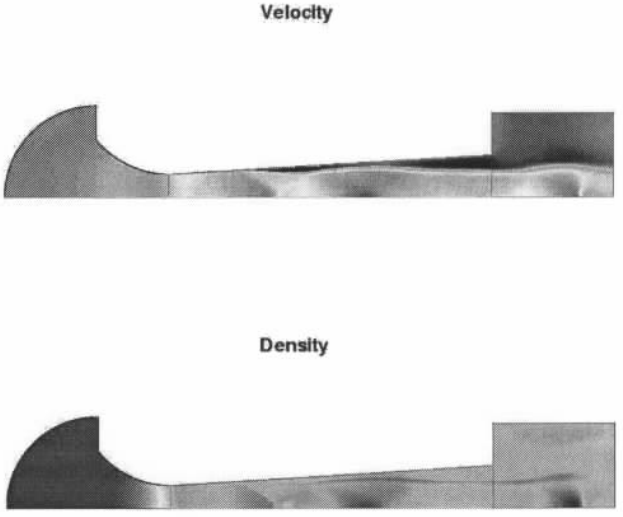

Figure 4: Resulting velocity and density countours.

As the exit pressure was still too large for a disturbance-free outflow (the pressure ratio of a corresponding well matched nozzle was approximately $p_{out}/p_0 = 0.02$ or about 10-times smaller), there were large fluctuations of the jet as it exits the nozzle.A system of oblique shocks with a Mach-stem shock at the center line formed, with the obligatory Mach-tripple point clearly distinguishable.The first oblique shock caused a separation of the flow at the wall. The separation point was not stationary, moving periodically in axial direction.Its mean location was approximately $D_{throat} = D^*$ downstream of the nozzle throat without ever reaching the throat itself.Outside of the nozzle, a fairly strong normal shock developed, again moving axially.The resulting shear layer can be seen considering both the velocity and the density. The flow structure, in particular within the wall shear layer, should be kept in mind during the following boundary layer stability considerations, as all the theories dealing with transition from laminar to turbulent flow are not valid in separated flow regions.

The resulting flow fields for the larger Reynolds

number of $Re_{ISO} = 4.15 \cdot 10^6$ were very similar, with a somewhat larger extent of the separation.They are not shown here due to space limitations.

IV. LOCATION OF TRANSITION

The above flow fields were analyzed using a separate evaluation computer program.The determination of the location of the transition was carried out in several steps:

- the various boundary layer thicknesses were determined
- the corresponding Reynolds numbers were computed
- the different shape factors were calculated
- finally, according to some semi-empirical criteria, the critical Reynolds numbers were compared with the local Reynolds numbers

Below, each of the steps will be explained in some more detail.

4.1 Boundary layer thickness

There are several definitions of the boundary layer thickness that are being used in the literature. These have to be kept strictly apart.The most commonly used, and most useless is the simple boundary layer thickness δ that is, actually strictly speaking, not defined at all.Many times, it is assumed that δ is found by the first occurance of $\frac{u}{U_e} \geq 0.99$ where u is the local velocity parallel to the wall and U_e is the velocity at the edge of the boundary layer. The problem in the case of the Venturi nozzle is that a) U_e is not known apriori and b) the velocity outside the boundary changes as a function of the radius.However, the knowledge of the velocity U_e is essential for the further considerations.Several approaches were tested, with mixed results. Finally, the method that worked the best consisted of two steps:
1) δ and U_e were estimated by assuming that the boundary layer edge was reached when $\frac{u'}{y'} \leq 5$, with $u' = \frac{u}{a_0}$ and $y' = \frac{y}{l_0}$. a_0 and l_0 are reference values at stagnation conditions.
2) more accurate estimate of δ was obtained by assuming that outside the boundary layer the convective terms in the Navier Stokes equations are much larger than the viscous terms. This means that

$$C = \frac{1}{Re_0} \cdot \frac{\mu \frac{\partial^2 u'}{\partial y'^2}}{\rho_\infty{}' U_e{}' \frac{\partial U_e{}'}{\partial x'}} \leq 0.005 \qquad (2)$$

The Reynolds number Re_0 will be explained in the following section. After finding the simple boundary layer thickness δ and, in particular, the edge velocity U_e, it is possible to determine the displacement thickness δ_1 and the momentum thickness δ_2. They are defined as

$$\delta_1 = \int_0^\infty \left(1 - \frac{\rho u}{\rho_e U_e}\right) dy \qquad (3)$$

$$\delta_2 = \int_0^\infty \frac{\rho u}{\rho_e U_e} \left(1 - \frac{u}{U_e}\right) dy \qquad (4)$$

It should be noticed that, according to Schlichting [22], $\delta_1 \approx 0.36\delta$ and $\delta_2 \approx 0.1366\delta$. Useful will be also so called shape factors, defined as

$$\Lambda = \frac{\delta^2}{\nu} \cdot \frac{\partial U_e}{\partial x} \qquad (5)$$

$$K = \frac{{\delta_2}^2}{\nu} \cdot \frac{\partial U_e}{\partial x} \qquad (6)$$

A further shape factor is defined as $H_{12} = \frac{\delta_1}{\delta_2}$; the present work, however, makes no use of it.
The resulting displacement thickness for the case $Re_{ISO} = 8.75 \cdot 10^5$ is displayed in Fig.5. The displacement thickness is plotted along the nozzle wall starting from the sharp corner in the inflow section of the nozzle. Immediately after the sharp corner, the flow is mildly separated, causing a significant increase of the displacement thickness. Then, the flow strongly accelarates due to a favourable pressure gradient. Accordingly, the boundary layer thickness decreases.Shortly before reaching the throat,it starts increasing again, as the favourable pressure gradient becommes smaller. The throat is located at $\frac{s}{D^*} = 1.71$. At this location, the displacement thickness displays a spike due to the discontinuous first derivative

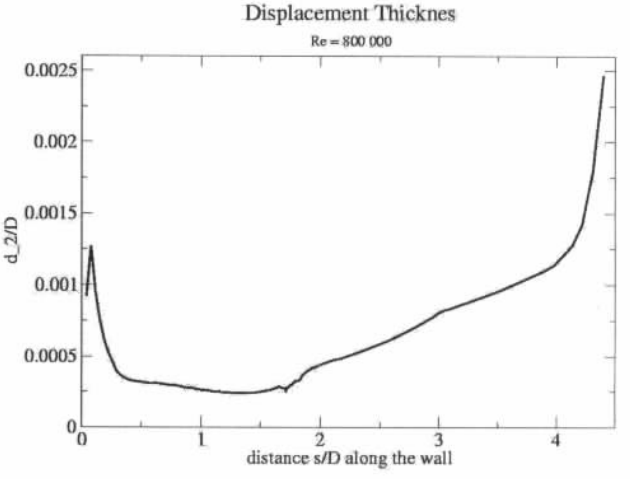

Figure 5: Displacement thickness along the nozzle wall, $Re_{ISO} = 8.75 \cdot 10^5$.

of the nozzle wall shape.Thereafter, the δ_1 rises steadily, until getting closer to the flow separation at approximately $\frac{s}{D^*} = 4$. Downstream of this $\frac{s}{D^*}$, the oblique shock induces an adverse pressure gradient that rsults in a significantly higher displacement thickness. The curve stops at separation. Noticable and important for the subsequent computations is the somewhat irregular shape of the δ_1-curve caused by the local charakter of its numerical determination. The velocity profile $U_e = f(\frac{s}{D^*})$, not shown here, has even more oscillatory tendency, leading to problems in the computation of the shape factors Λ and K. Although smoothing has been applied to the velocity profile, the resulting shape factors are strongly oscillating. More work could be invested into a better smoothing scheme for both U_e and δ_2 needed for the determination of the critical Reynolds numbers.

4.2 Which Reynolds number?

The surprisingly large number of Reynolds number definitions might be confusing, making a few remarks necessary. The most widely used Reynolds number is given by the ISO 9300 standard as $Re_{ISO} = \frac{\rho^* a^* D^*}{\mu_0}$. In the first authors opinion, this choice is not logical as it uses the stagnation value of the dynamic viscous coefficient μ_0. More logical would be the critical Reynolds number $Re_{D^*} = \frac{\rho^* a^* D^*}{\mu^*}$. Both of these Reynolds numbers are global, having no meaning for the local conditions in the boundary layer. Any considerations of the boundary layer development along the wall will have to use some Reynolds number that is function of the coordinate along the wall. Very fequently, the Reynolds number based on the simple distance from the leading edge $Re_x = \frac{\rho_e U_e x}{\mu}$ was employed in the BL-theory.In the BL-stability considerations,the Reynolds number based on one of the thicknesses δ, δ_1 or δ_2 has been in frequent use. The summary of the Reynolds numbers is given below.

- $Re_{ISO} = \frac{\rho a^* D^*}{\mu_0}$
- $Re_{D^*} = \frac{\rho a^* D^*}{\mu^*}$
- $Re_x = \frac{\rho_e U_e x}{\mu_e}$
- $Re_\delta = \frac{\rho_e U_e \delta}{\mu_e}$
- $Re_{\delta_1} = \frac{\rho_e U_e \delta_1}{\mu_e}$
- $Re_{\delta_2} = \frac{\rho_e U_e \delta_2}{\mu_e}$
- $Re_0 = \frac{\rho_0 a_0 l_0}{\mu_0}$

The last Reynolds number is based on the stagnation properties and was used to nondimensionalize the governing equations. It ensures the correct Re_{ISO} or Re_{D^*} for an orbitrary grid size.

4.3 Transition

Several methods for the determination of the location of transition can be found in the literature. In the present work, it was decided to select an approach that was simple yet gave results that were in reasonable agreement with the experimental results as well as general experience. It has been observed experimentally that the location of the transition depends on the free stream turbulence level outside the boundary layer as well as on some local boundary layer parameters that can be correlated to the Tollmien-Schlichting stability theory. Consequently, most of the transition theories attempt to find a critical Reynolds number (mostly $Re_{\delta_2,crit}$ based on the displacement thickness) that is a function of the free stream turbulence intensity Tu given in percent and one of the shape factors. It is then assumed that when the local Reynolds number Re_{δ_2} exceeds the critical Reynolds number $Re_{\delta_2,crit}$ the transition occures.

One of the simplest methods of finding the critical Reynolds number is offered by Schlichting [22]. He gives a graphical corellation between the critical Reynolds number $Re_{\delta,crit}$ and the shape factor Λ. This relation has been put into an analytical form $Re_{\delta,crit} = F(\Lambda)$ by using a general relaxation method. However,although the shape factor is defined between +12 for highly accelerated flows and -12 for separation due to adverse pressure gradient, the range of Λ given in [22] does not exceed ± 6. The shape factor Λ is subject to fairly strong fluctuations due to the problems discussed above, easilly reaching the maximum value of +12, making the determination of $Re_{\delta,crit}$ impossible. Clearly, this method was not well suited for the present problem.

Another approach,tailored specifically to internal turbomachinery problems, has been introduced by Mayle and Schulz [23]. Without going into the details of their derivations, the resulting relationship for the critical Reynolds number can be formulated as

$$Re_{\delta_2,crit} = 400 \cdot (Tu)^{-0.625} \qquad (7)$$

This approach worked better, since the momentum thickness δ_2 experiences much smaller oscillations than the boundary layer thickness δ. Besides, in contrast to the formulation given in [22], it depends on the turbulence intensity Tu. It is, however, independent of the local conditions, such as the pressure gradient or shape factor. The resulting critical Reynolds number is therefore constant along the wall and its value is too high.

The method that worked the best in the present case was developed by Abu-Ghannam and Shaw [24]. Here, the critical Reynolds number is correlated to both, Tu and the shape factor K through

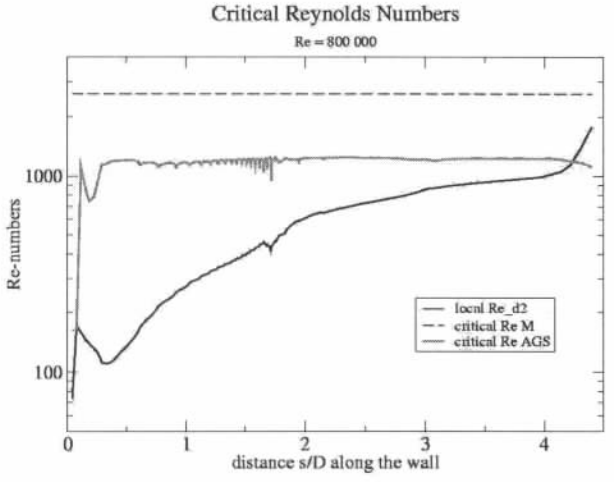

Figure 6: Critical Reynolds numbers compared to the local Re_{δ_2}.

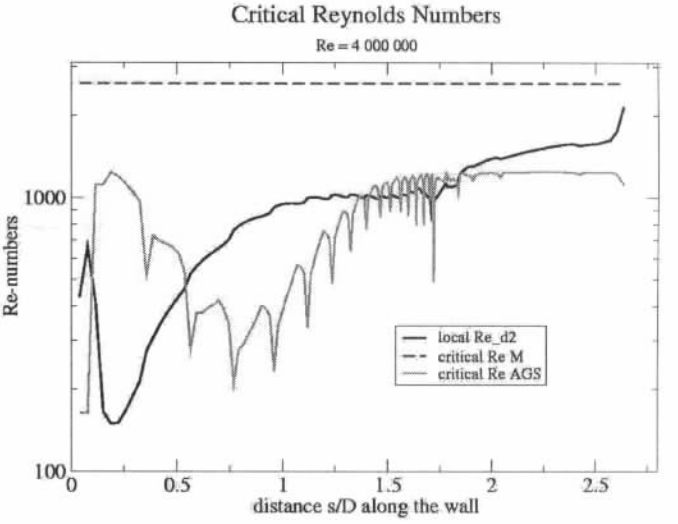

Figure 7: Critical Reynolds numbers compared to the local Re_{δ_2}.

an empirical function F(K):

$$\mathrm{Re}_{\delta_2,crit} = 163 + \exp\left(F(K) - \left(\frac{F(K)}{6.91}Tu\right)\right)$$

$$\mathrm{F(K)} = 6.91 + 12.75 \cdot K + 63.64 \cdot K^2 \; ; \; for K < 0$$

$$\mathrm{F(K)} = 6.91 + 2.48 \cdot K - 12.27 \cdot K^2 \; ; \; for K > 0$$

Although the calculated critical Reynolds number was showing some oscillations, these were much weaker that in the case of the Schlichting method. More significantly, the resulting location of the transition agreed qualitatively with the experimental investigations.

V. RESULTS

All three methods of predicting the existance and location of the transition have been applied to the two flow cases discussed above. These were interesting in regards to the transition phenomenon, since the case of the lower Reynolds number $Re_{ISO} = 8.75 \cdot 10^5$ is just at the lower range of the transitional Reynolds numbers, with the transition possibly located downstream of the throat due to the smooth walls of the nozzle. On the other hand, the second case at $Re_{ISO} = 4.15 \cdot 10^6$ is well in the turbulent region and should indicate early transition well ahead of the throat. In both computations, the turbulence intensity in the inflow was assumed to be $Tu = 4\%$.

The two more useful critical Reynolds numbers, $Re_{\delta_2,crit,M}$ due to [23] and $Re_{\delta_2,crit,ABS}$ according to Abu-Ghannam and Shaw are compared to the local Reynolds number based on the momentum thickness Re_{δ_2} in Fig. 6 for the case of $Re_{ISO} = 8.75 \cdot 10^5$. The local Reynolds number follows closely the trend set by the displacement thickness shown in Fig. 5 for the same Re_{ISO}. Considering the Abu-Ghannam-Shaw $Re_{\delta_2,crit,ABS}$, the transition will occure at approximately $\frac{s}{D^*} = 4.25$, being well downstream of the throat. The flow rate will be given by the laminar relationship in equation (1). The $Re_{\delta_2,crit,M}$ fails to predict any transition.

.

The same plot is shown in Fig. 7 for the higher Reynolds number $Re_{ISO} = 4.15 \cdot 10^6$. In the case of the higher Reynolds number, the flow separates earlier, at approximately $\frac{s}{D^*} = 2.75$. More importantly, however, the critical Reynolds number becomes smaller than the local Reynolds number well ahead of the throat, at about $\frac{s}{D^*} = 0.55$. Clearly, the flow in the throat will be turbulent, and consequently the C_D-coefficient will be obtained from equation (1) with $a = -0.2$.

VI. CONCLUSIONS

In the present work, the suspected transition of the boundary layer from laminar to turbulent has been investigated. To this end, the flow field in a Venturi nozzle shaped according to the ISO-standard 9300 has been simulated. After the converged results were obtained, the possibility of transition was investigated using three transional models. Only one of them, the Abu-Ghannam-Shaw approach, worked properly and predicted the correct trend observed experimentally. At flow conditions corresponding to $Re_{ISO} = 8.75 \cdot 10^5$, the transition was determined to be well downstream of the throat, not effecting the flow rate. On the other hand, at the higher reynolds number

of $Re_{ISO} = 4.15 \cdot 10^6$, the transition was predicted to be in the intake part of the nozzle, influencing the flow rate as expected.

In the next future, the Abu-Ghannam-Shaw approach will be applied to real gase flows in nozzles under high pressure metering natural gas.

References

[1] von Lavante, E. and Grönner, J., "Semiimplicit Schemes for Solving the Navier-Stokes Equations", 9th GAMM Conference, Lausanne, Notes on Numerical Fluid Mechanics, Vieweg, 1992.

[2] Norton, R. J. G., "Prediction of the Installed Performance of 2-dimensional Exhaust Nozzles", AIAA Paper 87-0245.

[3] Roe, P. L., "Characteristic Based Schemes for the Euler Equations", A Numerical Review of Fluid Mechanics, pp. 337-365, 1986.

[4] B. Nath, H. Dietrich, "Compteur étalon automatisé à tubes de Venturi fonctionnant en zone critique pour l'étalonnage de débitmètres ou de compteurs volumétrique." 8e Congrès International de Métrologie "Métrologie 97", 20.10.-23.10.97, Besançon, France.

[5] Ishibashi, M., and Takamoto, M., "Discharge Coefficient of Superaccurate Critical Nozzle at Pressurized Condition", Proccedings of the 4th Int. Symposium on Fluid Flow Measurement, Denver, USA, June 1999.

[6] Dietrich, H., Nath, B., and von Lavante, E., "High Accuracy Test Rig for Gas Flows from 0.01 m^3/h up to 25,000 m^3/h" Proceedings of the IMEKO-XV Congress, Osaka, Japan, June 1999.

[7] Ishibashi, M., and Takamoto, M., "Very Accurate Analytical Calculation of the Discharge Coefficient of Critical Venturi Nozzles with Laminar Boundary Layer", Proceedings of the FLUCOME97 Conference in Hayama, Japan, Sept. 1997.

[8] International Standard ISO 9300, "Measurement of gas flow by means of critical flow Venturi nozzles", First Edition, Beuth, Berlin 1990.

[9] von Lavante, E., Nath, B. and Dietrich, H., "Effects of Instabilities on Flow Rates in Small Sonic Nozzles", Proceedings of the 9th Int. Conference on Flow Measurement FLOMEKO'98, Lund, 1998.

[10] Ishibashi, M., von Lavante, E. and Takamoto, M., "Quasi- Nonintrusive Measurement of Flow Velocity Field in a Critical Nozzle", Proceedings of ASME FEDSM'00, June 11-15, Boston, 2000.

[11] Wendt, G., Ph.D. Thesis, University of Essen, Germany, 2000.

[12] von Lavante, E., El-Milligui, A. and Warda, H., "Simulation of Unsteady Flows Using Personal Computers", The 3rd Int. Congress on Fluid Mechanics, Cairo, 1990.

[13] Steger, J. L., "Implicit, Finite-Difference Simulation of Flow about Arbitrary Geometries", AIAA Journal, Vol. 16, No. 7, 1978.

[14] von Lavante, E., El-Miligui, A., Cannizzaro, F. E., and Warda, H. A., "Simple Explicit Upwind Schemes for Solving Compressible Flows", Proceedings of the 8th GAMM Conference on Numerical Methods in Fluid Mechanics, Delft, 1990.

[15] Nakao, Shin-ichi, "Choking Phenomenon of Sonic Venturi Nozzles on Low Reynolds Numbers", Proceedings of the 9th Int. Conference on Flow Measurement FLOMEKO'98, Lund, 1998.

[16] Wendt, G. and von Lavante, E., "Influence of Surface Roughness on the Flow Rate Behavior of Small Critical Venturi Nozzles", Proceedings of the 10th Int. Conference on Flow Measurement FLOMEKO'2000, Salvador, 2000.

[17] Ishibashi, M. and Takamoto, M., "Very Accurate Analytical Calculation of the Discharge Coefficient of Critical Venturi Nozzles with Laminar Boundary Layer", Proceedings of the FLUCOME97, Hayama, Japan, Sept. 1997.

[18] von Lavante, E., Zachcial, A., Zeitz, D., Nath, B. and Dietrich, H., "Effects of Various Geometric Parameters on the Flow Behavior in Sonic Nozzles", Proceedings of the 10th Int. Conference on Flow Measurement FLOMEKO'2000, Salvador, Brasil 2000.

[19] von Lavante, E., Zachcial, A., Färber, J., Nath, B. and Dietrich, H., "Simulation of Unsteady Effects in Sonic Nozzles Used for Flow Metering", Proceedings of the 8th Int. Symposium on Computational Fluid Dynamics, Bremen, Germany Sept. 1999.

[20] Vallet J. P., Windenbeger, C., Vulovic, F. and Bourd, R., "Improvement of Themodynamic Calculations Used for the Flow Rate of Sonic Nozzles", Proceedings of the 10th Int. Conference on Flow Measurement FLOMEKO'2000, Salvador, Brasil 2000.

[21] Ishibashi, M., "Proposal of Fluid Dynamical Standard (FDS) for Gas Flow-Rate", 5th ISFFM, Arlington, USA, April 7-10 2002.

[22] Schlichting, H.,"Boundary Layer Theory", McGraw-Hill, 7th edition, 1979.

[23] Mayle, R. E. and Schulz, A.,"The Path to Predicting Bypass Transition", Journal of Turbomachinery, 119(3), pp. 405-411, 1997.

[24] Abu-Ghannam, B. J. and Shaw, R.,"Natural Transition of Boundary Layers - The Effect of Turbulence, Pressure Gradient and Flow History", IMechE, Vol. 22, No. 5, 1980.